Available online at www.sciencedirect.com
SCIENCE DIRECT
Lithos 90 (2006) 77–91
LITHOS
www.elsevier.com/locate/lithos

High pressure petrogenesis of Mg-rich garnet pyroxenites from Mir kimberlite, Russia

M.F. Roden [a,*], A.E. Patiño-Douce [a], E. Jagoutz [b], E.E. Laz'ko [c]

[a] Department of Geology, University of Georgia, Athens, GA 30602, USA
[b] Department Kosmochemie, Max Planck Institut fur Chemie, Mainz, Germany
[c] ALROSA Stock Company, Moscow, 117447, Russia

Received 11 February 2005; accepted 16 January 2006
Available online 15 March 2006

Abstract

Some Mg-rich garnet pyroxenites from the Mir kimberlite, Siberia, have garnets containing oriented arrays of diopside, rutile+diopside or rutile+Mg-rich ilmenite inclusions. Present mineral compositions require storing of the pyroxenites in the mantle lithosphere at relatively low pressures and temperatures (2.5–3.7 GPa, 680–820 °C). However, the arrays of mineral inclusions are attributed to exsolution from an original higher pressure and/or temperature garnet. Garnets containing arrays of diopside or diopside and rutile exsolved at least a small amount (<1%) of a majoritic component in the form of mineral inclusions but may have exsolved much more of the majoritic component (up to 20%) in the form of pyroxene distributed along grain boundaries. The original garnets probably formed at pressures near or above 5 GPa and may represent phenocrysts formed in high pressure magmas that were injected into the continental lithosphere as crystal-melt mixtures. Alternatively, these pyroxenites may have been tectonically or diapirically emplaced into the continental lithosphere as advocated for ultrahigh pressure peridotites in some crustal terranes. In either case, subducted oceanic lithosphere may have been the source material. Previously documented isotopic disequilibrium between garnet and diopside in one of the Mir pyroxenites requires storage of the pyroxenite in the continental lithosphere for several hundred million years.

Keywords: Majorite; Garnet; Kimberlite; Xenolith; Garnet pyroxenite

1. Introduction

Garnet is a key mineral constituent of the upper mantle and its composition systematically changes as a function of pressure and temperature. At very high pressures (>5 GPa), garnet can incorporate a pyroxene (i.e., majoritic) component and become supersilicic due to the substitution of Si for Al in the octahedral site (e.g., Akaogi and Akimoto, 1979; Irifune, 1987; Draper et al., 2003). Such supersilicic garnets are preserved as inclusions in diamonds and charge balance in these garnets is maintained by coupled substitution of Na in the X site and/or coupled substitution of Ca, Fe and Mg in the Y site (Akaogi and Akimoto, 1979; Moore and Gurney, 1985; Ono and Yasuda, 1996). Elements such as Ti and P may also substitute in very high pressure garnets with or without excess Si (e.g., Thompson, 1975; Bishop et al., 1976; Zhang et al., 2003). Some garnets found in ultrahigh pressure metamorphic terranes or in kimberlite xenoliths have mineral inclusions arrayed along {111}

* Corresponding author. Tel.: +1 706 542 2416; fax: +1 706 542 2425.
E-mail address: mroden@gly.uga.edu (M.F. Roden).

0024-4937/$ - see front matter © 2006 Elsevier B.V. All rights reserved.
doi:10.1016/j.lithos.2006.01.005

planes that appear to have formed by exsolution of components due to a decrease in pressure and/or temperature. For example, garnets from peridotite and eclogite xenoliths from Africa contain pyroxene lamellae suggested to have formed by exsolution from an originally majoritic garnet stabilized at pressures greater than 10 GPa (Haggerty and Sautter, 1990; Deines and Haggerty, 2000). Other garnets with inclusions of pyroxene (Western Gneiss Region, Norway, Van Roermund and Drury, 1998) are thought to have formed as majoritic garnets at pressures of approximately 6 GPa. Yet other garnets from the Western Gneiss Region contain inclusions of the titanium oxides (rutile and ilmenite); some rutile inclusions are associated with pyroxene inclusions and the assemblage may document the breakdown of a high pressure Ti-rich garnet (Van Roermund et al., 2000a). Similar occurrences of Si- and Ti-rich mineral inclusions in garnet were recently reported from the Sulu ultrahigh pressure terrane (Ye et al., 2000; Zhang and Liou, 2003) and the North Qaidam ultrahigh pressure terrane (Song et al., 2004). In the Sulu locality, apatite needles occur in some garnets.

Laz'ko (1979) noted the occurrence of oriented ilmenite, Cr-spinel and rutile needles in garnets from Mir and Udachnaya kimberlites, Siberia (see Sobolev et al., 2004, for a recent map of the Yakutian or Siberian kimberlite fields); he interpreted these inclusions to have formed by exsolution. In this paper, we report new mineral analyses for garnets and associated pyroxenes in Mg-rich garnet pyroxenites from Mir as well as for inclusions of clinopyroxene, ilmenite or rutile, which form triangular arrays in the host garnet. We also report on image analyses of these arrays, which constrain the relative volumes of inclusions and host garnet. The inclusion assemblages are clinopyroxene alone, clinopyroxene plus rutile and rutile plus Mg-rich ilmenite. We interpret these inclusions to have formed by exsolution from a high pressure garnet, following Haggerty and Sautter (1990). However, the discrete minerals in the pyroxenites have compositions similar to minerals from relatively low temperature, granular lherzolites, which suggests that the pyroxenites last equilibrated at relatively low pressures and temperatures in the continental lithosphere (as did the granular lherzolites, e.g., Roden et al., 1999). Nonetheless, the exsolved mineral inclusions in garnets of the pyroxenites testify to a very high pressure origin ($P > 5.0$ GPa).

2. Sample description

The six samples with apparent exsolution features within garnets are all garnet-rich pyroxenites. These pyroxenites are relatively unstrained and coarse grained; typical grain size is in the range 3 mm to 1 cm diameter and the grains have straight to curved boundaries. All the samples contain two pyroxenes but the relative proportion of these phases varies greatly; thus, the rocks range from clinopyroxene-bearing garnet orthopyroxenites to orthopyroxene-bearing garnet clinopyroxenites. Minor amounts of olivine occur in half the samples. In addition to olivine, some of the samples contain small (< 1 mm), discrete grains of rutile, ilmenite or phlogopite. In some samples, relatively small pyroxenes are distributed along grain boundaries of larger garnets (Fig. 1); this texture is similar to that illustrated by Van Roermund and Drury (1998) for garnet nodules from the Western Gneiss Region of Norway. Alteration is common in the xenoliths but variable; typically, olivine and orthopyroxene are replaced by pale reddish to clear, fibrous pseudomorphs, which based on optical properties, are mixtures of talc,

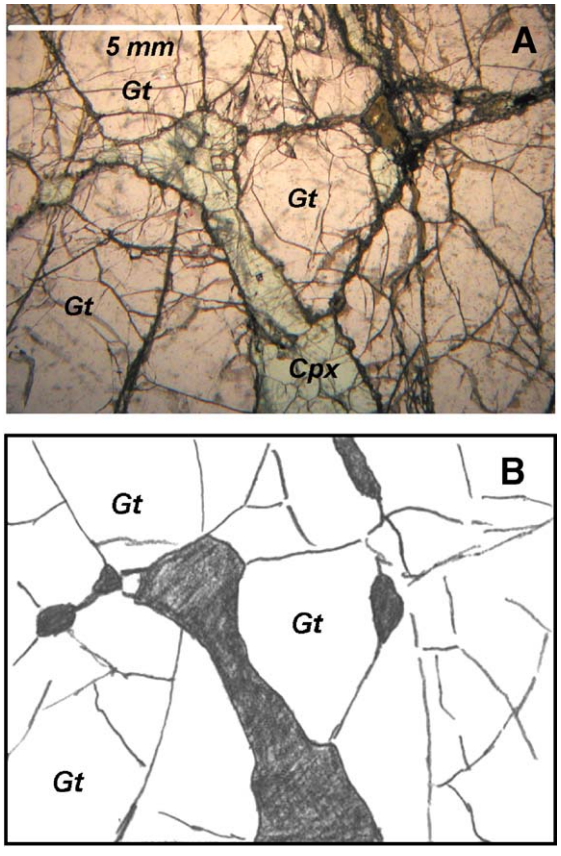

Fig. 1. (A) Clinopyroxene (Cpx, pale green) distributed along the grain boundaries of garnet (Gt, pale pink) in pyroxenite TM-90. (B) Sketch of same photomicrograph showing all clinopyroxene grains as black. (For interpretation of the references to colour in this figure legend, the reader is referred to the web version of this article.)

serpentine and very fine grained iron oxides or hydroxides. The primary silicates may be completely replaced or small remnants may be preserved as islands amongst the replacement minerals. Thin carbonate or carbonate + phlogopite veins occur in two xenoliths and cross cutting relations show that these veins predate the wholesale replacement of olivine and orthopyroxene. Consequently, metasomatism may have affected the bulk rock compositions, but there is no observable effect on the exsolution textures we discuss here.

Mineral inclusions are common in the silicate minerals except olivine. Garnets contain small rods of pyroxene, needles of rutile and plates of ilmenite, which form triangular arrays in thin section (Fig. 2). In some examples, additional inclusion orientations exist and may project partially out of the plane of the thin section (Fig. 2C,D). Typically, pyroxene grains contain thin lamellae (<0.1–0.8 mm long) of the other pyroxene as well as the oxide phase found as lamellae in the garnet of the rock. Such lamellae occur even in small pyroxenes distributed along grain boundaries between large garnets (e.g., Fig. 1). Moreover, the oxide phase that occurs as lamella in garnet commonly occurs as discrete grains along grain boundaries—perhaps indicating an origin

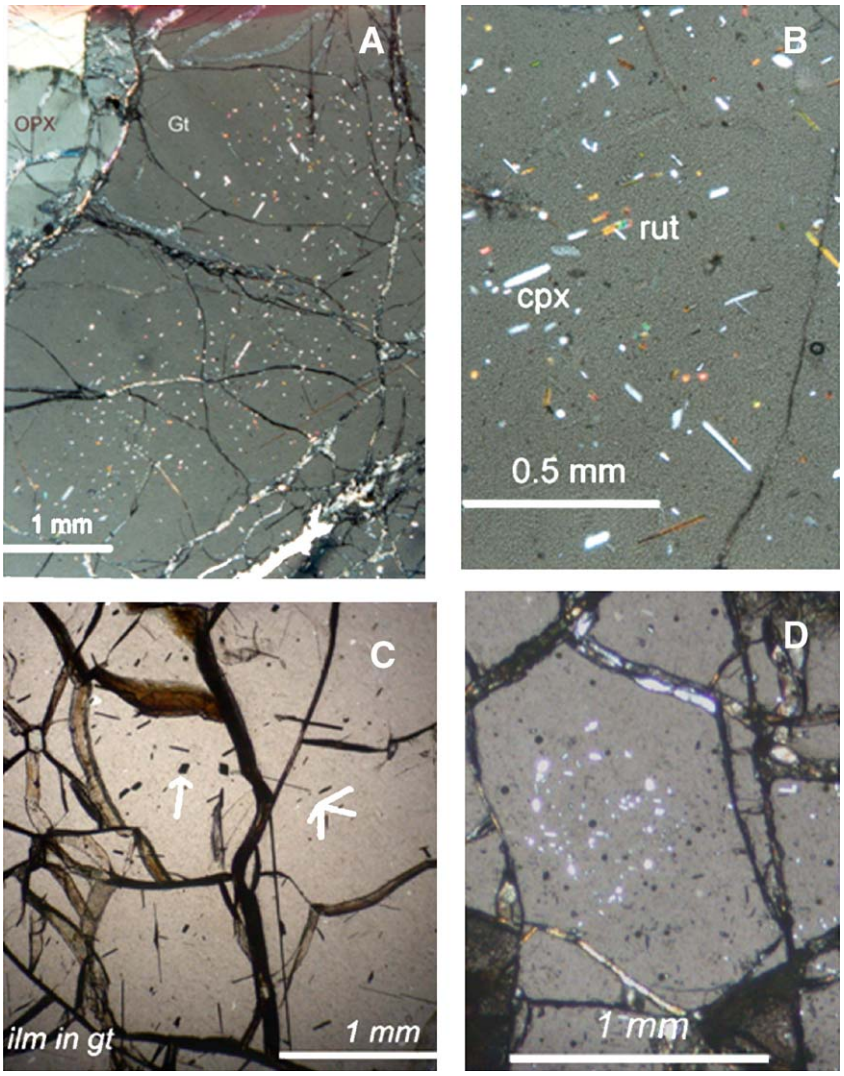

Fig. 2. Mineral inclusion arrays in garnets of pyroxenite xenoliths from Mir. (A, B) Inclusion arrays of diopside and rutile in garnet of TM-90 viewed at two magnifications. Note the clear garnet grain rim adjacent to orthopyroxene in Fig. 1A. (C) Inclusion array of ilmenite and rutile in TM-91. On the right side of the photomicrograph, white lines are drawn parallel to the long dimension of neighboring ilmenite lamellae. The relatively short white line is parallel to an orientation that is only poorly developed. The arrow points to a rhombus-shaped basal section of ilmenite which defines a fifth orientation of lamellae. (D) Inclusion array of stubby diopside rods in garnet of TM-53.

by exsolution for these discrete oxide grains. In garnet, the platelets and needles of rutile and ilmenite range up to 0.5 mm long, whereas the stubby rods of pyroxene are shorter, ranging up to 0.3 mm long. These latter grains, when their long axes are parallel, commonly go to extinction simultaneously, indicating that the grains have similar crystallographic orientations. Many of the rutile inclusions have inclined extinction; this unusual optical behavior (rutile is tetragonal and usually has parallel extinction) was also noted by Van Roermund et al. (2000a) and Song et al. (2004) for rutile inclusions in ultrahigh pressure garnets from Western Gneiss Region, Norway and North Qaidam, China. Griffin et al. (1971) attributed such anomalous extinction in rutile to elongation parallel to a pyramid face. Inclusion arrays tend to be concentrated in the interior of the garnets and in some samples the garnets have an inclusion-free rim 0.3–0.7 mm wide around inclusion-rich centers (Fig. 2A). Garnets in a given section can be inclusion-rich or inclusion-free but this distinction may be an artifact of the position of the section surface in the garnet. The volume of the inclusions relative to that of the host garnet is small: for example, in pyroxenite TM-90 (Fig. 2A,B), the inclusions of rutile and diopside comprise approximately 1% of the host garnet according to our image analysis of back-scattered electron images as discussed below.

The mineral assemblage of the inclusion arrays varies from sample to sample: in two samples (TM-25, TM-90), the garnets contain diopside and rutile; in two other samples (TM-53, TM-126), the garnets contain diopside only; and, in two other samples (TM-91, TM-149), the garnets contain rutile and ilmenite but no pyroxene. These inclusion arrays are similar to the arrays attributed to exsolution by Haggerty and Sautter (1990) in xenoliths from the Jagersfontein kimberlite. As described below, the garnets in all samples are compositionally similar and pyrope-rich but exhibit compositional ranges in TiO_2, FeO, MnO and especially Cr_2O_3. Small differences in garnet compositions correlate with the nature of the inclusion arrays: garnets that contain oxide inclusions are richer in TiO_2 (~0.12 wt.% versus 0.05 wt.%) compared to garnets that have clinopyroxene inclusions only, and those that contain ilmenite are richer in FeO (8.3–10.2 wt.%) compared to garnets that lack ilmenite (6.6 wt.%–8.2 wt.%).

One curious aspect of the diopside inclusion array in sample TM-53 is that the median size of a clinopyroxene inclusion in the array varies from place to place in a thin section or even in a single garnet: one array within a garnet may be characterized by relatively large inclusions, while another area is characterized by very small inclusions barely resolvable with the microscope. Van Roermund et al. (2001) reported a similar observation for orthopyroxene inclusions in garnets of ultramafic bodies from the Western Gneiss Region, Norway.

3. Analytical methods

Mineral compositions were determined using a JEOL electron microprobe at the University of Georgia following methods outlined previously (Roden and Shimizu, 1993). Typical operating conditions were 15 kV accelerating voltage, 15 nA beam current and an analytical spot size of approximately 1 μm diameter. Elemental X-ray intensities in unknowns were measured for 10 s and compared to those in natural or synthetic mineral standards and converted to abundances using phi(rho Z) corrections following Armstrong (1988). Analytical precision and accuracy were monitored by repeated analyses of mineral standards treated as unknowns. In particular, the Smithsonian standards, Cr-augite (NMNH 164905) and Johnstown hypersthene (USNM 746) were each analyzed 12 times over the course of the study—roughly comparable to the number of analyses for a given mineral reported here. Precision of our mean analyses of these two mineral standards shows that the precision for major elements is in the range of 1–2% (1 S.D.) for most major elements (>2 wt.% oxide) but somewhat worse for FeO (3%). Our major element means are within 2% of the published values (Jarosewich et al., 1980, 1987) except our Al_2O_3 content for the Cr-augite is 4% less (7.71 wt.% versus 8.03 wt.%) than the published value. In contrast, our measured Al_2O_3 content for the Johnstown pyroxene, 1.25 wt.%, is indistinguishable from the published value (1.23 wt.%). Intriguingly, Jarosewich et al. (1987) reported a wet chemical analysis of the Cr augite standard in which the Al_2O_3 content was 7.59 wt.%; consequently, our relatively low measured Al_2O_3 contents could reflect inhomogeneity in the Cr-augite grains.

We used image analysis software (Scion Image available from the National Institute of Health) to estimate the volumes of included phases in garnet. Photo mosaics of back-scattered electron images were created for garnet interiors in TM-90 (rutile and diopside inclusions), TM-126 (diopside inclusions) and TM-91 (ilmenite and rutile inclusions). For each sample, two to four garnets were imaged; total area imaged ranged from 0.7 mm^2 (TM-126) to more than 5 mm^2 (for TM-90, TM-91). The relatively small area imaged for TM-126 is a result of the small individual image size needed to accurately analyze the areas of the small diopside

inclusions. The same software was also used to estimate the amount of interstitial pyroxene between garnet grains over an area of 250 mm^2 of TM-90.

4. Results

4.1. Mineral compositions

Representative mineral compositions are presented in Tables 1–3. The silicates are Mg-rich: Mg/(Mg+Fe) ratios of enstatite and diopside are 0.92–0.95 and 0.92–0.97, respectively, and olivine found in two samples, TM-25 and TM-149, is also Mg-rich (Fo_{92-93}). The silicates are generally unzoned and compositionally similar to those found in granular, low temperature lherzolites from Mir (e.g., Roden et al., 1999). Consequently, the silicates in these exsolved garnet pyroxenites are quite distinct from the more Fe-rich silicates of eclogites from Mir (Fig. 3).

Garnets are predominantly pyrope and have a range of Cr_2O_3 (0.2–2.9 wt.%, Table 1) and CaO contents (3.5 to 5 wt.%), which correlate positively with each other (Fig. 4). The Ca/Mg/Fe ratios are consistent with buffering of garnet compositions by diopside plus orthopyroxene (Table 1; Boyd, 1970). Grain homogeneity is particularly striking in the case of garnet: inclusion-free grain rims are compositionally indistinguishable from inclusion-rich grain centers or nearly so—garnets in TM-25 have slightly more Fe-rich and Mg-poor rims compared to their grain centers (Table 1). Garnet compositions and the nature of the inclusion arrays show some correlation: garnets that contain oxide minerals in the arrays are richer in TiO_2 (~0.12 wt.% versus 0.05 wt.%) compared to garnets that have clinopyroxene inclusions only, and those that contain ilmenite are richer in FeO (8.3–10.2 wt.%) compared to garnets that lack ilmenite (6.6 wt.%–8.2 wt.%).

Table 1
Representative garnet analyses

Sample	TM-25	TM-25	TM-25	TM-53	TM-90	TM-90	TM-90	TM-91	TM-126	TM-149
n	33	9	4	5	17	9	3	7	19	17
Comment	Average garnet	Garnet interior	Garnet rim	Average garnet	Average garnet	Garnet interior	Garnet rim	Average garnet	Average garnet	Average garnet
SiO_2	42.00	41.99	41.91	41.77	42.37	42.25	41.90	41.62	41.85	42.00
TiO_2	0.12	0.09	0.10	ND	0.10	0.11	0.10	0.12	ND	0.14
Al_2O_3	21.90	21.98	21.97	23.42	23.73	23.83	23.77	23.57	22.51	22.77
MgO	20.25	20.39	20.02	21.63	21.90	22.02	21.92	20.52	20.65	20.86
FeO	8.23	8.08	8.46	6.87	6.62	6.55	6.59	10.22	7.77	8.30
CaO	4.93	4.90	4.94	4.63	4.49	4.59	4.30	3.52	4.85	4.30
MnO	0.40	0.41	0.47	0.27	0.19	0.19	0.24	0.25	0.33	0.31
Cr_2O_3	2.85	2.79	2.92	1.24	0.96	0.97	1.05	0.22	2.27	1.23
Total	100.68	100.61	100.78	99.83	100.40	100.50	99.87	100.04	100.24	99.90
Cations normalized to 12 oxygens										
Si	2.983	2.981	2.978	2.955	2.971	2.959	2.954	2.965	2.971	2.985
Ti	0.006	0.005	0.005		0.005	0.006	0.005	0.006		0.008
Al	1.833	1.839	1.840	1.952	1.961	1.967	1.975	1.979	1.884	1.908
Mg	2.143	2.158	2.120	2.280	2.289	2.299	2.304	2.178	2.186	2.211
Fe	0.489	0.480	0.503	0.406	0.388	0.384	0.388	0.609	0.462	0.493
Ca	0.375	0.373	0.376	0.351	0.337	0.344	0.325	0.268	0.369	0.327
Mn	0.024	0.024	0.029	0.016	0.012	0.011	0.014	0.015	0.020	0.018
Cr	0.160	0.157	0.164	0.070	0.053	0.053	0.058	0.013	0.127	0.069
Sum	8.014	8.016	8.015	8.032	8.016	8.024	8.024	8.033	8.022	8.019
Endmember proportions (mol%)										
Uvarovite	7.9	7.7	8.1	3.4	2.6	2.6	2.9	0.6	6.3	3.4
Pyrope	70.7	71.1	70.0	74.7	75.6	75.7	76.0	70.9	72.0	72.5
Spess	0.8	0.8	0.9	0.5	0.4	0.4	0.5	0.5	0.7	0.6
Gross	4.4	4.5	4.3	8.1	8.5	8.7	7.8	8.1	5.9	7.3
Alm	16.1	15.8	16.6	13.3	12.8	12.6	12.8	19.8	15.2	16.2

ND = not detected.

Table 2
Representative pyroxene analyses

Sample	TM-25	TM-53	TM-90	TM-90	TM-91	TM-126	TM-126	TM-149	TM-25	TM-25	TM-53	TM-53	TM-90	TM-90	TM-90	TM-91	TM-126	TM-126	TM-149
Mineral	opx	opx	opx	opx	opx	opx	opx	opx	cpx	cpx	cpx	cpx	cpx	cpx	cpx	cpx	cpx	cpx	cpx
n	3	3	17	5	14	6	3	6	7	6	4	3	21	3	8	7	4	4	12
Comment	Average discrete grain	Average discrete grain	Average discrete grain	Average lamella in cpx	Average discrete grain	Average discrete grain	Average lamella in cpx	Average discrete grain	Average discrete grain	Average lamella in gt	Average discrete grain	Average lamella in gt	Average discrete grain	Average lamella in opx	Average lamella in gt	Average discrete grain	Average discrete grain	Average lamella in gt	Average discrete grain interior
SiO_2	58.24	57.30	58.35	58.29	57.57	58.00	58.11	57.20	54.80	54.36	54.73	54.89	54.70	54.52	54.82	54.96	54.92	54.89	54.09
TiO_2	ND	ND	ND	ND	ND	ND	ND	ND	0.23	0.18	ND	ND	0.24	0.24	0.22	0.36	ND	ND	0.33
Al_2O_3	0.88	0.69	0.60	0.60	0.50	0.53	0.49	1.08	3.50	2.96	2.41	2.27	3.04	3.21	2.49	6.14	2.50	1.91	5.47
MgO	36.85	37.17	37.18	37.46	35.65	36.55	36.80	36.22	15.55	16.13	16.77	17.15	16.58	16.72	17.01	13.93	16.27	17.01	14.56
FeO	4.13	4.15	3.75	3.70	5.86	4.42	4.34	4.45	1.33	1.59	1.10	1.39	0.98	1.07	1.08	2.04	1.57	1.56	1.28
CaO	0.15	0.19	0.19	0.25	0.15	0.19	0.34	0.11	20.94	20.96	22.18	22.41	21.69	20.98	22.12	18.55	21.69	22.45	20.17
Na_2O	ND	ND	ND	ND	ND	ND	ND	ND	2.27	2.13	1.69	1.55	1.85	2.10	1.68	3.79	1.88	1.49	3.06
Cr_2O_3	0.17	ND	ND	ND	ND	0.16	0.19	0.19	1.96	1.98	0.90	0.76	0.60	0.79	0.69	0.25	1.07	0.96	1.26
Total	100.40	99.61	100.07	100.31	99.73	99.84	100.28	99.25	100.58	100.28	99.77	100.42	99.68	99.62	100.11	100.02	99.89	100.27	100.22
Cations normalized to 6 oxygens																			
Si	1.975	1.962	1.980	1.974	1.982	1.981	1.978	1.966	1.964	1.959	1.975	1.971	1.972	1.967	1.972	1.967	1.982	1.978	1.941
Ti									0.006	0.005		0.002	0.007	0.007	0.006	0.010			0.009
Al	0.035	0.028	0.024	0.024	0.020	0.021	0.020	0.044	0.148	0.126	0.102	0.096	0.129	0.136	0.106	0.259	0.106	0.081	0.231
Mg	1.862	1.897	1.880	1.891	1.823	1.860	1.867	1.856	0.830	0.866	0.902	0.918	0.891	0.899	0.912	0.743	0.875	0.913	0.779
Fe	0.117	0.119	0.106	0.105	0.168	0.126	0.124	0.128	0.040	0.048	0.033	0.042	0.030	0.032	0.032	0.061	0.047	0.047	0.038
Ca	0.005	0.007	0.007	0.009	0.006	0.007	0.012	0.004	0.804	0.809	0.858	0.862	0.838	0.811	0.853	0.711	0.838	0.867	0.775
Na									0.157	0.149	0.118	0.108	0.130	0.147	0.117	0.263	0.132	0.104	0.213
Cr	0.005					0.004	0.005	0.005	0.055	0.056	0.026	0.021	0.017	0.023	0.020	0.007	0.031	0.027	0.036
Sum	4.003	4.020	4.005	4.010	4.007	4.004	4.008	4.007	4.006	4.019	4.018	4.022	4.013	4.021	4.018	4.021	4.014	4.019	4.023
Mg#	94.1	94.1	94.6	94.7	91.6	93.7	93.8	93.6	95.4	94.8	96.4	95.6	96.8	96.5	96.6	92.4	94.9	95.1	95.3

ND = not detected.

Table 3
Representative rutile and ilmenite analyses

Sample	TM-25	TM-90	TM-149	TM-149		TM-91	TM-91	TM-149
Mineral	Rutile	Rutile	Rutile	Rutile		Ilmenite	Ilmenite	Ilmenite
n	3	3	2	2		8	2	2
Comment	Average lamella in garnet	Average lamella in garnet	Average lamella in gt	Average discrete grain		Average lamella in gt	Discrete ilmenite	Average lamella in gt
SiO_2	0.07	0.07	0.13	ND	SiO_2	ND	ND	0.09
TiO_2	97.89	97.07	97.72	99.11	TiO_2	57.62	58.34	58.40
Al_2O_3	ND	0.20	ND	ND	Al_2O_3	0.26	0.19	0.16
MgO	0.07	ND	ND	ND	MgO	13.50	13.55	16.88
Fe_2O_3	0.51	0.55	0.62	ND	FeO	27.26	26.92	22.26
CaO	0.22	0.19	0.24	ND	Fe_2O_3	0.42	0.00	1.08
Cr_2O_3	0.80	1.23	0.99	0.78	CaO	0.08	ND	0.17
Total	99.58	99.32	100.25	99.89	MnO	ND	0.26	0.16
Cations normalized to 2 oxygens					Cr_2O_3	ND	0.20	0.83
Si	0.001	0.001	0.002		NiO	0.50	0.59	NA
Ti	0.986	0.981	0.983	0.992	Total	99.64	100.05	100.04
Al		0.003			*Cations normalized to 6 oxygens*			
Mg	0.001				Si			0.004
Fe^{3+}	0.005	0.006	0.006		Ti	1.984	1.998	1.957
Ca	0.003	0.003	0.003		Al	0.014	0.010	0.009
Cr	0.008	0.013	0.010	0.008	Mg	0.922	0.920	1.121
Sum	1.005	1.007	1.006	1.002	Fe^{2+}	1.044	1.025	0.830
					Fe^{3+}	0.014	0.000	0.036
					Ca	0.004		0.008
					Mn		0.010	0.006
					Cr		0.007	0.029
					Ni	0.018	0.022	
					Sum	4.001	3.993	4.001

All Fe reported as Fe^{3+} in rutile; Fe^{3+} calculated from charge balance in ilmenite.
ND = not detected.
NA = not analyzed.

Pyroxenes are unzoned and inclusions of pyroxene in other minerals are similar to or identical in composition to discrete grains of pyroxene. The orthopyroxene is nearly pure enstatite with only minor amounts of ferrosilite and tschermak components (Al_2O_3 0.5–1.1 wt.%, Table 2). Most clinopyroxenes are diopsides albeit with significant amounts of jadeite in solid solution; two of the pyroxenes have about 25% jadeite component (TM-91, TM-149) and can be classified as omphacites following Morimoto et al. (1988). Pyroxenes are generally unzoned and homogeneous in a given sample; the only exception is that diopside occurring as an inclusion in garnet has 1–3% lower jadeite content than discrete diopside occurring outside garnet in the same pyroxenite (e.g., TM-90, TM-53, TM-126, Table 2). Curiously, this is opposite to the observations of Song et al. (2004) who found that clinopyroxene rods in garnet had higher jadeite content than matrix pyroxene.

Rutile is nearly pure TiO_2 but contains measurable Cr and Fe as is common in mantle-derived rutiles (Haggerty, 1991). We also report measurable CaO in grains occurring as inclusions in garnet and diopside; however, this CaO is likely due to secondary fluorescence from the silicate host given the absence of measurable CaO in discrete grains of rutile in TM-149 (Table 3). Ilmenites are quite Mg-rich with Fe/Mg atomic ratios in the range, 0.7–1.3, and, where Ni was measured, quite Ni-rich (Table 3) as well. Stoichiometric calculations indicate that there is little or no hematite in solution. The ilmenities in TM-91 and TM-149 are distinguished from most kimberlitic ilmenites (Wyatt et al., 2004) by their very low ferric iron contents and in the case of the ilmenite from TM-149, high MgO content.

4.2. Image analysis

In the three samples where inclusion volumes in garnet were measured, the volume of included minerals is relatively small, less than 1%. In TM-90, the garnet contained 0.5% diopside and 0.09% rutile; in TM-126, the garnet contained 0.7% diopside; and, in TM-91, the garnet contained 0.4% ilmenite and 0.01% rutile.

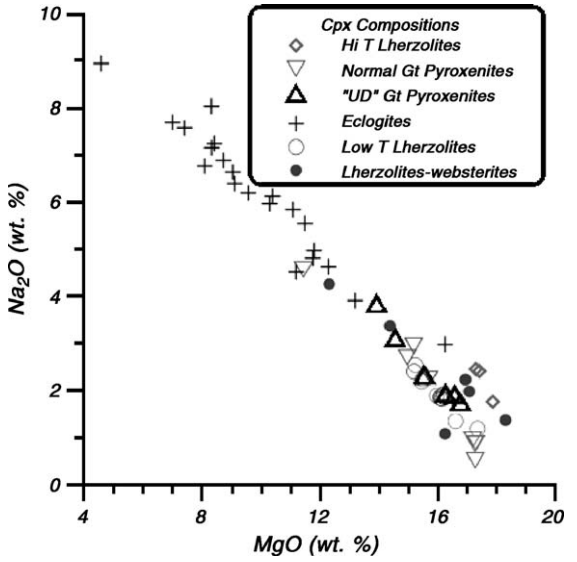

Fig. 3. Soda and MgO contents of clinopyroxenes from peridotites and eclogites from Mir. "UD" garnet pyroxenites contain garnets with oriented arrays of mineral inclusions attributed to exsolution (the subject of this paper), whereas the other pyroxenites contain garnets without such mineral arrays. Data are taken from Agashev et al. (2001), Beard et al. (1996), McCulloch (1986), Roden et al. (1999), Sobolev (1977), Zhuralev et al. (1991) and this paper. The undifferentiated lherzolite–websterite data are from Sobolev (1977).

The volume of grain boundary pyroxene was also measured in sample TM-90 (Fig. 1) given the suggestion by Haggerty and Sautter (1990) that grain boundary exsolution was important in similar xenoliths from the Jagersfontein kimberlite. Only a limited amount of sample was available and, thus, the results are somewhat uncertain. Given that caveat, we measured 13% diopside and 7% orthopyroxene distributed along grain boundaries of host garnet in an area of 250 mm^2.

5. Discussion

5.1. High pressure–temperature substitutions

The mineral inclusion arrays in garnet form triangular patterns in plan view (see Fig. 2) which Haggerty and Sautter (1990) suggested was consistent with exsolution along {111} planes in garnet. Van Roermund et al. (2000b) found patterns of pyroxene needles in garnet consistent with exsolution along {110} as well as {111} planes in garnet. Close inspection of Fig. 2C shows an example of ilmenite lamellae that are oriented in at least five directions including rhombus-shaped basal sections which is consistent with exsolution textures described by Van Roermund et al. (2000b). Following Haggerty and Sautter (1990), we believe that these arrays have formed by exsolution because of the crystallographic control of the orientation of the inclusions, and the extensive experimental evidence showing solid solution between garnet and pyroxene at high pressures (e.g., Draper et al., 2003).

One of the mineral inclusions, diopside, forms a high pressure solid solution with garnet (e.g., Akaogi and Akimoto, 1979). Although experimental evidence showing solid solution between ilmenite–geikielite and garnet is lacking, there is solution of $MgSiO_3$ in garnet when it coexists with silicate ilmenite, $MgSiO_3$, at very high ($P > 18$ GPa) pressures (Gasparik, 1992). Moreover, substitution of ilmenite–geikielite could occur in garnet via $MTiAl_{-2}$ where M is Fe^{2+} or Mg. Exsolution of the third type of mineral inclusion, rutile, from garnet poses stoichiometric problems which are explored further below.

The six Mir pyroxenites under discussion contain three distinct inclusion assemblages in garnet: diopside, diopside + rutile and ilmenite + rutile. The first assemblage is the easiest to interpret. Garnets from TM-53 and TM-126 exhibit arrays of diopside alone, and the compositions of the exsolved diopside in the two samples are similar (Table 2). These pyroxene compositions can be recast into a garnet molecule, $X_3Y_2Z_3O_{12}$, by normalizing the cations to 12 oxygens and assigning the cations sequentially, first to pyrope/uvarovite, then to a component based on the coupled substitution of Na and Si (Sobolev and Lavrent'ev, 1971), and finally

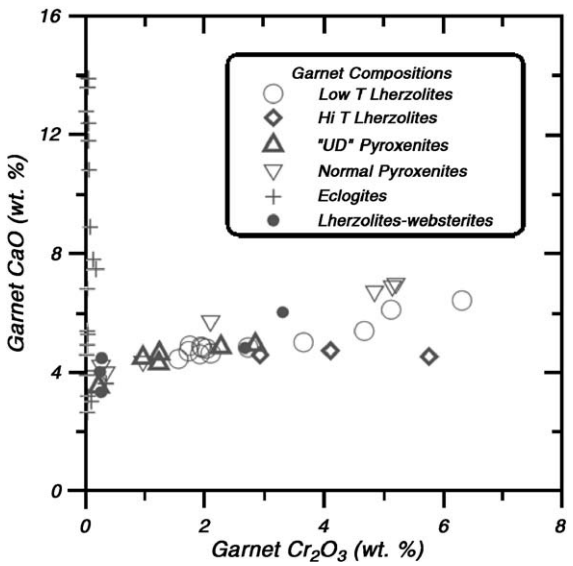

Fig. 4. Calcium oxide and Cr_2O_3 contents of garnets from peridotites and eclogites from Mir. Symbols and data sources are the same as in Fig. 2.

assigning the remaining cations to a majoritic component. This order of assignment consumes all available Al in the first step and maximizes the amount of "normal", i.e., pyrope+uvarovite, garnet components with Al in the octahedral site. The results show that the clinopyroxene mineral inclusions predominantly (~80%) reflect a majoritic substitution, $MSiAl_{-2}$, where M is Fe^{2+}, Mg or Ca, with lesser amounts of pyrope+uvarovite (~10%) and coupled substitution of Na and Si ($NaSi(MAl)_{-1}$, ~10%). The original garnet composition can be calculated based on the volume (0.7%) of exsolved diopside in garnets of TM-126, which we measured by image analysis. The effect of reconstituting the garnet is small: this volume of diopside converted to a mass equivalent increases the Si content by only 0.002 Si per 12 oxygens (Table 4). Nonetheless, the visually abundant diopside inclusions in garnets of TM-126 (Fig. 2D) demonstrate that the garnets formed at pressures and temperatures high enough so that the majoritic substitution was effective.

Our approach to estimating the amount of exsolved diopside in the garnets is conservative. Other authors who examined similar garnets in pyroxenites and peridotites also found low volumes of exsolved pyroxene in garnet cores (e.g., Van Roermund and Drury, 1998; Song et al., 2004), but argued that exsolution of pyroxene from garnet could be extended to the grain boundary area (e.g., Haggerty and Sautter, 1990; Van Roermund and Drury, 1998). This type of exsolution also may have been important in the Mir pyroxenites as evidenced by the distribution of small pyroxene grains with large surface areas along grain boundaries of much larger garnets in some pyroxenites (Fig. 1), garnet grain rims which are free from mineral inclusions (Fig. 2A) and the occurrence of discrete oxide grains along grain boundaries which have the same composition as oxide inclusions in garnet (Table 3). Intriguingly, some of the small, interstitial pyroxene grains contain exsolution lamellae of oxides and pyroxene; if these small pyroxene grains formed by exsolution, then the process that triggered exsolution may have been episodic or prolonged. Using image analysis of a thin section of TM-90, we estimated that as much as 20% of the original garnet may have exsolved as diopside and enstatite along grain boundaries. If this idea is correct, then the original garnet was majorite-rich with 3.15 silicon atoms per 12 oxygens (Table 4).

Table 4
Recalculated garnets

Sample	TM-126 [a]	TM-91 [a]	TM-90 [a]	TM-90 [b]
SiO_2	41.88	41.41	42.26	44.82
TiO_2		0.41	0.21	0.20
Al_2O_3	22.47	23.45	23.71	19.69
MgO	20.64	20.48	21.98	22.33
FeO	7.76	10.31	6.52	5.67
CaO	4.89	3.50	4.66	6.42
MnO	0.33	0.25	0.19	0.15
Cr_2O_3	2.27	0.22	0.96	0.86
Na_2O	0.00		0.01	0.23
Total	100.23	100.04	100.49	100.37
Cations normalized to 12				
Si	2.975	2.953	2.961	3.145
Ti	0.000	0.022	0.011	0.011
Al	1.881	1.971	1.958	1.628
Mg	2.186	2.177	2.295	2.335
Fe	0.461	0.615	0.382	0.333
Ca	0.372	0.268	0.350	0.483
Mn	0.020	0.015	0.011	0.009
Cr	0.127	0.012	0.053	0.048
Na	0.000	0.000	0.001	0.031
Sum	8.021	8.033	8.023	8.022

[a] Garnets+mineral inclusions.
[b] Garnet+mineral inclusions+discrete pyroxene.

Experimental evidence (summarized in Draper et al., 2003) indicates that the substitution of Si in the octahedral sites depends primarily on pressure but is also sensitive to temperature and mineral assemblage. For example, the presence of clinopyroxene (which is likely in the clinopyroxene-bearing assemblages under discussion) may increase the pressure at which majorite substitution is initiated. A compilation of 7 GPa experiments (Ono and Yasuda, 1996; Bertka and Fei, 1997; Walther, 1998) shows that increasing temperature at constant pressure causes an increase in the amount of majoritic component in garnet and in the CMAS system, Gasparik (1990) found that majorite substitution in pyrope was moderately temperature dependent at pressures ranging from 4 to 16 GPa. Van Roermund et al. (2000a) used experimental data to draw temperature-dependent majorite isopleths for garnet in pressure–temperature space. All these interpretations of experimental data show that, at constant pressure, the amount of majorite substitution increases as temperature increases.

Clinopyroxene-saturated experiments show that the majoritic substitution is initiated in garnet at pressures greater than 5–7 GPa (Draper et al., 2003); these pressures may represent the minimum pressure for the formation of the original garnet in TM-53 and TM-126. Clinopyroxene saturated experiments at pressures of 5 GPa or lower do not show temperature dependency (Akaogi and Akimoto, 1979; Yasuda and Fujii, 1994; Ono and Yasuda, 1996; Bertka and Fei, 1997; Walther, 1998); consequently, the effect of temperature on our estimates of a minimum pressure is uncertain. If the

garnets formed at pressures lower than 5 GPa, then the temperatures were probably at least 1400 °C following the synthesis of Van Roermund et al. (2000a). If, on the other hand, some or all of the interstitial pyroxene formed by exsolution, then the garnets may have formed at much higher pressures. For example, if the garnet in TM-90 is recalculated assuming the interstitial pyroxene formed by exsolution, then it contains 3.15 silicon atoms per 12 oxygens (Table 4), and may have formed at pressures as high as 15 GPa (Draper et al., 2003) or within the transition zone as argued for similar xenoliths by Sautter et al. (1991). Consistent with this idea is the discovery by Sobolev et al. (2004) of majoritic garnet inclusions in Yakutian diamonds; these garnets have up to up to 3.13 silicon atoms per 12 oxygens.

Two of the pyroxenites have oriented inclusions of diopside and rutile but the exsolution of these two minerals poses a stoichiometric dilemma: regardless of the exact ratio of diopside to rutile, it is impossible to recast the cations of these minerals into a garnet formula without creating cation vacancies (see also discussion in Van Roermund et al., 2000a). Zhang et al. (2003) showed that Ti will substitute in garnet at high pressure (>5 GPa) via a $CaTiAl_{-2}$ substitution and they argued that rutile+diopside inclusions would be produced by exsolution during decompression of a titaniferous, majoritic garnet. However, in the exsolution reaction that they proposed, free silica in the form of quartz or coesite is consumed. In the Mir garnet pyroxenites free quartz is lacking and, unless it was completely consumed during exsolution, some other mechanism is needed to explain the stoichiometry of the exsolved phases. In the sample we studied most intensively, TM-90, we found the diopside/rutile lamellae ratio to be approximately 5:1. Recasting these two minerals as garnet using this ratio, results in a garnet component with only 7.7 cations (normalized to 12 oxygens) and excess Si, 3.3 Si per 12 oxygens. Consequently, the mineral inclusions represent a titaniferous (16 wt. % TiO_2), majoritic garnet component with a cation deficiency in the octahedral site, which contains only 1.5 cations. When the pyroxene and rutile lamellae are combined with the host garnet in the proportions consistent with our image analysis, the reconstituted garnet has about twice as much TiO_2 (0.22 versus 0.11 wt.%), slightly more CaO (an increase of 0.07 wt.% CaO) and marginally more Si (an increase of 0.002 Si per 12 oxygens) compared to the host garnet (Table 4). Nonetheless, the bulk composition of the inclusion array in TM-90 (as calculated above) clearly shows that they represent a majoritic component. We conclude, as we did for TM-126, and using similar reasoning, that the original garnet formed at pressures of at least 5 GPa. Additionally, if the interstitial pyroxene formed by exsolution, then the original garnet was quite majorite-rich (Table 4) and must have formed at much higher pressures as noted above.

The Ti-rich composition of the exsolved majoritic component in the garnet of TM-90 is intriguing. Bell and Rossman (1992a,b) reported a range of <1 to 200 ppm H_2O in mantle-derived garnets as well as a positive correlation between H_2O and TiO_2 in garnets from the subcontinental mantle of South Africa; Matsyuk et al. (1998) reported a similar range in H_2O contents in garnets from the Siberian mantle lithosphere including some garnets from Mir. Geiger et al. (1991) produced synthetic pyropes with H_2O contents of up to 0.07 wt.%. Based on analyses of OH-bearing garnet megacrysts from the Monastery kimberlite, Bell et al. (2004) suggested that some of the OH in garnet may be associated with Ti. Intriguingly, Aines and Rossman (1984) and Bell and Rossman (1992a) reported that garnet xenocrysts from ultramafic diatremes of the Colorado Plateau were particularly rich in water and many of these garnets contain rutile needles "oriented in geometric patterns" (Hunter and Smith, 1981). Moreover, Wang et al. (1999) noted that rutile inclusions in these same garnets were hydrous and the amount of water correlated with the water content of the host garnet. Consequently, a possible explanation for the high oxygen/cation ratio of the exsolved phases in Mir garnets such as those in pyroxenite TM-90 is that some oxygen was associated with H in the original garnet structure.

Two of the pyroxenites contain oriented inclusions of ilmenite and rutile in garnet and, if these inclusions formed by exsolution, then they pose the same stoichiometric dilemma as the diopside and rutile inclusions. However, in TM-91, we found by image analysis that the ratio of ilmenite to rutile lamella was approximately 75:1; calculating a garnet molecule using this mass ratio and the analyses in Table 3 results in a garnet molecule of the form $M_3MTiTi_3O_{12}$ (M=Fe or Mg), which has 7.97 cations per 12 oxygens, i.e., no significant cation vacancies. To our knowledge, no experimental data exist that are relevant to the substitution of Mg-rich ilmenite into garnet, but this may be another high pressure and temperature substitution. The observation that the ilmenite-bearing garnets are more iron-rich than the clinopyroxene- or clinopyroxene+rutile-bearing garnets suggests that bulk composition is important in determining whether rutile or ilmenite exsolves from the garnet.

Table 5
Results of thermobarometric calculations (P and T in GPa and °C respectively)

Sample	P^a	T^b	P^c	T^d	Garnet inclusion assemblage
TM-25	2.5	730	2.5	649	Diopside+rutile
TM-53	3.2	794	3.2	674	Diopside
TM-90	3.7	817	3.7	681	Diopside+rutile
TM-91	3.6	790	3.6	805	Ilmenite+rutile
TM-126	3.5	804	3.5	780	Diopside
TM-149	2.1	676	2.1	639	Ilmenite+rutile

[a] Calculated pressure using Al-in-opx barometer of Brey and Kohler (1990).
[b] Calculated temperature using the Ca-in-opx thermometer of Brey and Kohler (1990).
[c] Assumed pressure for calculation of temperature based on garnet–diopside equilibria.
[d] Calculated temperature using the garnet–clinopyroxene thermometer of Krogh Ravna (2000).

5.2. Lower pressure–temperature evolution

The observation that mineral compositions in the studied pyroxenites are nearly indistinguishable from mineral compositions in granular lherzolites that equilibrated at relatively low pressures and temperatures (Figs. 3 and 4) suggest that, regardless of the history of the pyroxenites, they last equilibrated at upper mantle conditions. The close approach to equilibrium is documented by the homogeneity of the pyroxene within each rock: compositions of pyroxene in discrete grains are nearly identical to compositions of lamellae within garnet and the other pyroxene (Table 2). Previously, we utilized the thermobarometer of Brey and Kohler (1990) to estimate equilibration pressures and temperatures for two of the pyroxenites (TM-149, 2.1 GPa, 676 °C; TM-90, 3.0 GPa, 670 °C, Roden et al., 1999), and these pressures and temperatures are similar to those for granular garnet peridotites from Mir and coarse lherzolites from the Udachnaya pipe (Boyd et al., 1997; Roden et al., 1999). Hence, we conclude that these two pyroxenites were stored in the mantle lithosphere prior to incorporation in kimberlite. Haggerty and Sautter (1990) reached similar conclusions in the case of xenoliths from Jagersfontein that exhibited similar inclusion arrays in garnet.

All six of the pyroxenites under discussion contain the assemblage, garnet+enstatite+diopside±olivine and, thus, the thermobarometers of Brey and Kohler (1990) can be used to estimate equilibration conditions. Smith (1999) suggested that the Ca-in-orthopyroxene thermometer (Brey and Kohler, 1990) may be more accurate at temperatures less 900 °C; hence, we utilized this thermometer in conjunction with the garnet–orthopyroxene barometer of Brey and Kohler (1990) to estimate equilibration pressures and temperatures for the six pyroxenites (Table 5), given the relatively low estimated temperatures for pyroxenites TM-90 and TM-149 previously estimated (see above). We also recalculated the equilibration temperatures and pressures for the relatively low temperature, granular lherzolites from Mir, and the results are displayed in Fig. 5. All the pyroxenites equilibrated at relatively low pressures and temperatures (2.5 to 3.7 GPa and 676 to 817 °C, Table

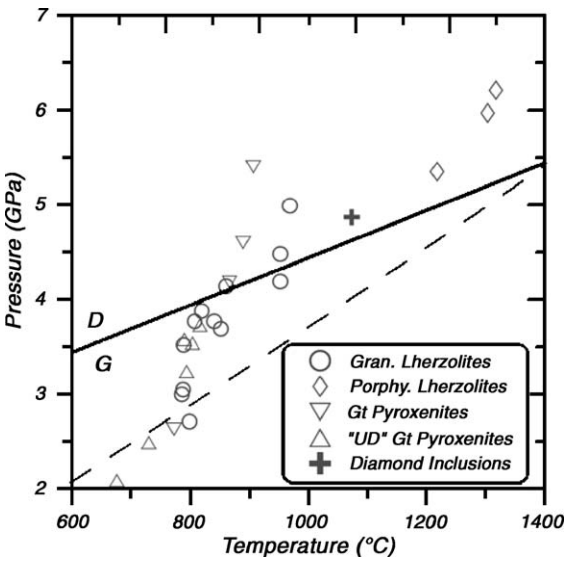

Fig. 5. Results of thermobarometric calculations for peridotites and pyroxenites from Mir. "UD" garnet pyroxenites contain garnets with oriented arrays of mineral inclusions attributed to exsolution, whereas the other pyroxenites contain garnets without such mineral arrays. Calculations utilized the Ca-in-opx thermometer and orthopyroxene barometer of Brey and Kohler (1990) except for the diamond inclusion and porphyroclastic lherzolites where temperature was calculated utilizing the two pyroxene thermometer of Brey and Kohler (1990). Data for Mir xenoliths are taken from Sobolev (mineral inclusions in diamond A-34, 1977), Zhuralev et al. (1991), Roden et al. (1999), Agashev et al. (2001) and this paper. Diamond–graphite equilibrium (solid line) taken from Kennedy and Kennedy (1976); the dashed line represents a calculated conductive geotherm based on heat flow of 50 mW/m^2 and a two-layer crust (upper and lower) and upper mantle following Stein (1995) and Turcotte and Schubert (2002).

5), which are similar to those for the granular lherzolites from Mir (2.7 to 4.2 GPa and 786 to 953 °C). There is a tendency for the pyroxenites to yield somewhat lower pressures and temperatures but the ranges overlap (Fig. 5). Use of the garnet–clinopyroxene thermometer as calibrated by Ai (1994) and Krogh Ravna (2000) confirms the relatively low temperatures of equilibration (assuming a pressure consistent with the results from the Brey and Kohler barometer) for the six Mir garnet pyroxenites containing garnets with exsolution lamellae (Table 5).

Chemical homogeneity of minerals as well as abundant exsolution lamellae in the garnet and pyroxenes of these pyroxenites requires their residence at relatively low pressures and temperatures for some time. The length of this residence period is uncertain but was probably in excess of several hundred million years based on Nd isotope disequilibrium between phases in the pyroxenites: Roden et al. (1999) reported garnet–clinopyroxene "ages" of 814 Ma for TM-90 (this sample has rutile and diopside exsolution in garnet) and 533 Ma for TM-41, a garnet pyroxenite in which the garnet lacks abundant exsolution lamellae. More recently, Agashev et al. (2001) reported a 1.22 Ga garnet–clinopyroxene "age" for a websterite from Mir. It is unclear whether the garnets of this xenolith contain mineral inclusions although Agashev et al. (2001) noted that the garnets of the pyroxenites they examined commonly contained oriented rutile needles. An unambiguous interpretation of the meaning of these "ages" is not possible: these rocks were stored at high temperatures but below the closure temperature for Nd in diopside (Van Orman et al., 2002), and a simple time interpretation of the ages is probably not valid. The 500 Ma to 1200 Ga garnet–clinopyroxene ages minus the approximately 360 Ma age (Pearson et al., 1997) of the host kimberlite probably represent minimum low pressure storage times (i.e., 140–840 million years) for these pyroxenites; the magnitude of the storage times precludes a direct relationship between the host kimberlite and the pyroxenites. Intriguingly, the likely wallrocks for the pyroxenites, the low temperature garnet lherzolites from Mir, also commonly exhibit Nd isotopic disequilibrium. In these garnet lherzolites, garnet–clinopyroxene ages range from 800 Ma to 2 Ga (Pearson et al., 1995; Gunther and Jagoutz, 1997). Macdougall and Haggerty (1999) also reported mineral Nd isotope disequilibrium in African kimberlite xenoliths containing garnets with exsolution lamellae; they also concluded that these xenoliths had been stored at moderate pressures in the continental lithosphere for several hundred million years. Such Sm–Nd disequilibria between garnet and clinopyroxene are probably common in the relatively cold lithospheric mantle beneath relatively old and stable continental crust (e.g., Brueckner and Medaris, 1998).

Given the mineralogic, thermobarometric and isotopic data described above, garnet and perhaps pyroxene were emplaced in the continental lithosphere several hundred million years before host kimberlite magmatism. Ideas concerning the transport mechanism are speculative, but there appear to be three possible scenarios: crystallization from a very high temperature magma at relatively low (~3 GPa) pressures, tectonic or diapiric emplacement of pyroxenites derived from pressures of 5 GPa or more (path A, Fig. 6), or magmatic emplacement of garnet megacrysts formed at pressures of 5 GPa or more (path B, Fig. 6). The first possibility would require implausibly high temperatures (~1800 °C) given the modest (but poorly known) temperature dependency of the majorite substitution (e.g., Van Roermund et al., 2000a). The second model has been used to explain the presence of ultrahigh pressure peridotites

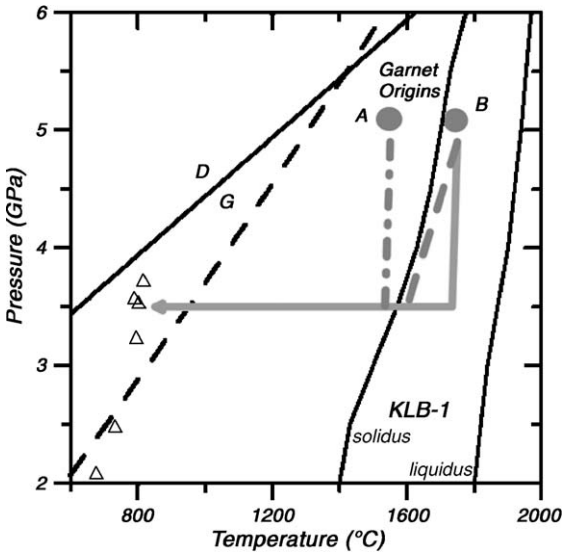

Fig. 6. Possible pressure–temperature paths for the high pressure garnets discussed in this paper. Path A is a subsolidus convective ascent from an initial state where pressure was at least 5 GPa and temperature was poorly constrained. Similar models have been advocated for ultrahigh pressure peridotites in crustal terranes as well as African xenoliths (e.g., Brueckner and Medaris, 2000; Haggerty and Sautter, 1990). Path B illustrates ascent via magmatic transport along an adiabatic path (grey solid line) or along a path where heat was lost to the surroundings or consumed by melting of entrained solids (grey dashed line). Diamond–graphite equilibria (black solid line) and 50 mW/m^2 conductive geotherm (black dashed line) are taken from Fig. 4 and the solidus and liquidus for peridotite KLB-1 are from Fei and Bertka (1999).

in crustal terranes (e.g., Brueckner and Medaris, 2000; Drury et al., 2001) as well as the emplacement of African kimberlite xenoliths into the continental mantle lithosphere (Haggerty and Sautter, 1990). This emplacement path (A in Fig. 6) could be consistent with a source in subducted lithosphere, but the data do not require it. Intriguingly, Sobolev et al. (2004) reported finding a majoritic garnet with a positive Eu anomaly as an inclusion in a Yakutian diamond—such an anomaly might reflect a protolith containing plagioclase such as subducted lithosphere.

An alternative explanation is that the garnets of the pyroxenites represent magmatic megacrysts that formed at pressures of 5 GPa or higher. These megacrysts could be carried upward by the host magma along an adiabatic or near-adiabatic path (B in Fig. 6) and injected into the lithosphere to form garnet pyroxenite dikes. Roden et al. (1999) reported relatively high Nd (25 ppm) and Sr (320 ppm) contents for the diopside of TM-90 and suggested that the pyroxenites might be accumulations from a kimberlitic melt; likewise, Macdougall and Haggerty (1999) reported high Sr contents (130–890 ppm) in clinopyroxene of African kimberlite xenoliths containing garnet with exsolution lamellae. Moreover, garnet is a liquidus or near-liquidus phase in MORB and kimberlite compositions at pressures above 5 GPa (Yasuda and Fujii, 1994; Mitchell, 2004) although in the kimberlite experiments the garnet was not majoritic. If the Mir xenoliths were transported upwards from depths of more than 150 km by an alkalic magma, relatively low magmatic density due to high volatile contents may have facilitated the rise of the magma. Moreover, high magmatic volatiles could have encouraged the crystallization of titaniferous, hydroxide-rich garnets given the Ti–OH association in mantle-derived garnets noted by Bell et al. (2004). The high volatile contents combined with relatively Ti-rich garnets, high Sr content of TM-90 diopside and the finding of a positive Eu anomaly in a majorite inclusion in diamond (Sobolev et al., 2004) all could be explained if the magmatic source included subducted oceanic lithosphere.

6. Conclusions

Exsolution textures in the garnets of the six garnet pyroxenites described in this paper testify to a high pressure petrogenesis. Thermobarometric calculations, in contrast, suggest that these pyroxenites equilibrated at relatively low pressures and temperatures (2.5–3.7 GPa, 680–820 °C) in the mantle lithosphere. Previously documented isotopic disequilibrium between garnet and clinopyroxene in one of these pyroxenites indicates a long residence time at relatively low temperatures and pressures, and this may be common in cratonic lithosphere (e.g., Gunther and Jagoutz, 1997; Brueckner and Medaris, 1998). The resemblance between these xenoliths and xenoliths from Jagersfontein, South Africa (Haggerty and Sautter, 1990; Sautter et al., 1991) is striking, and suggests that the preservation of very high pressure garnets in the mantle lithosphere may be widespread. The mechanism by which these high pressure minerals are emplaced into the lithosphere is difficult to infer given our inability to examine more than small xenolithic fragments. Plausible scenarios are (1) generation of relatively low density, hydrous magmas at depths of 150 km or more ($P > 5$ GPa)—these hydrous magmas carried suspended crystals and injected them into the mantle lithosphere; and (2) tectonic or diapiric emplacement of pyroxenite as advocated for some ultrahigh pressure peridotites found in crustal terranes. In either case, subducted oceanic lithosphere may have been an important source material.

Acknowledgements

This work has been supported at various times by the Max Planck Society, a NATO collaborative research grant, NSF and the University of Georgia. Thanks to Doug Smith and Steve Haggerty for their perceptive comments on an initial draft, Chris Fleisher for his invaluable help with the electron microprobe, Todd Watkins for editorial comments, and H. van Roermund and N. Sobolev for their constructive reviews.

References

Agashev, A.M., Watanabe, T., Kuligan, S.S., Pokhilenko, N.P., Orihashi, Y., 2001. Rb–Sr and Sm–Nd isotopes in garnet pyroxenite xenoliths from Siberian kimberlites: an insight into lithospheric mantle. J. Mineral. Petrol. Sci. 96, 7–18.

Ai, Y., 1994. A revision of the garnet–clinopyroxene Fe^{2+}–Mg exchange geothermometer. Contrib. Mineral. Petrol. 115, 467–473.

Aines, R.D., Rossman, G.R., 1984. Water content of mantle garnets. Geology 12, 720–723.

Akaogi, M., Akimoto, S., 1979. High pressure phase equilibria in a garnet lherzolite, with special reference to Mg^{2+}–Fe^{2+} partitioning among constituent minerals. Phys. Earth Planet. Inter. 19, 31–51.

Armstrong, J.T., 1988. Quantitative analysis of silicate and oxide minerals: a comparison of Monte Carlo, ZAF, and phi (rho Z) procedures. In: Newbury, D.E. (Ed.), Microbeam Analysis, pp. 239–246.

Beard, B.L., Fraracci, K.N., Taylor, L.A., Snyder, G.A., Clayton, R.A., Mayeda, T.K., Sobolev, N., 1996. Petrography and geochemistry of eclogites from the Mir kimberlite, Yakutia, Russia. Contrib. Mineral. Petrol. 125, 293–310.

Bell, D.R., Rossman, G.R., 1992a. Water in Earth's mantle: the role of nominally anhydrous minerals. Science 255, 1391–1397.

Bell, D.R., Rossman, G.R., 1992b. The distribution of hydroxyl in garnets from the subcontinental mantle of southern Africa. Contrib. Mineral. Petrol. 111, 161–178.

Bell, D.R., Rossman, G.R., Moore, R.O., 2004. Abundance and partitioning of OH in a high-pressure magmatic system: megacrysts from the Monastery kimberlite, South Africa. J. Petrol. 45, 1539–1564.

Bertka, C.M., Fei, Y., 1997. Mineralogy of the Martian interior up to core–mantle boundary pressures. J. Geophys. Res. 102 B, 5251–5264.

Bishop, F.C., Smith, J.V., Dawson, J.B., 1976. Na, P, Ti and coordination of Si in garnet from peridotite and eclogite xenoliths. Nature 260, 696–697.

Boyd, F.R., 1970. Garnet peridotites and the system $CaSiO_3$–$MgSiO_3$–Al_2O_3. In: Morgan, B.H. (Ed.), Fiftieth Anniversary Symposia: Mineralogy and Petrology of the Upper Mantle, Sulfides, Mineralogy and Geochemistry of Non-Marine Evaporites. Mineralogical Society of America Special Paper, vol. 3, pp. 63–76.

Boyd, F.R., Pokhilenko, N.P., Pearson, D.G., Mertzman, S.A., Sobolev, N.V., Finger, L.W., 1997. Composition of the Siberian cratonic mantle: evidence from Udachnaya peridotite xenoliths. Contrib. Mineral. Petrol. 128, 228–246.

Brey, G., Kohler, T., 1990. Geothermobarometry in four-phase lherzolites: II. New thermobarometers, and practical assessment of existing thermobarometers. J. Petrol. 31, 1353–1378.

Brueckner, H.K., Medaris, L.G., 1998. A tale of two orogens: the contrasting *T–P–t* history and geochemical evolution of mantle in high-and ultrahigh-pressure metamorphic terranes of the Norwegian Caledonides and Czech Variscides. Schweiz. Mineral. Petrogr. Mitt. 78, 293–307.

Brueckner, H.K., Medaris, L.G., 2000. A general model for the intrusion and evolution of 'mantle' garnet peridotites in high-pressure and ultra-high pressure metamorphic terranes. J. Metamorph. Geol. 18, 123–133.

Deines, P., Haggerty, S., 2000. Small-scale oxygen isotope variations and petrochemistry of ultradeep (>300 km) and transition zone xenoliths. Geochim. Cosmochim. Acta 64, 117–131.

Draper, D.S., Xirouchakis, D., Agee, C.B., 2003. Trace element partitioning between garnet and chondritic melt from 5 to 9 GPa: implications for the onset of the majorite transition in the Martian mantle. Phys. Earth Planet. Inter. 139, 149–169.

Drury, M.R., Van Roermund, H.L.M., Carswell, D.A., De Smet, J.H., Van Den Berg, A.P., Vlaar, N.J., 2001. Emplacement of deep upper-mantle rocks into cratonic lithosphere by convection and diapiric upwelling. J. Petrol. 42, 131–140.

Fei, Y., Bertka, C., 1999. Phase transitions in the Earth's mantle and mantle mineralogy. In: Fei, Y., Bertka, C., Mysen, B.O. (Eds.), Mantle Petrology: Field Observations and High-Pressure Experimentation, A Tribute to Francis, R. (Joe) Boyd. The Geochemical Society, Houston, TX, pp. 171–188.

Gasparik, T., 1990. Phase relations in the transition zone. J. Geophys. Res. 95 (B), 15751–15769.

Gasparik, T., 1992. Enstatite–jadeite join and its role in the Earth's mantle. Contrib. Mineral. Petrol. 111, 283–298.

Geiger, C.A., Langer, K., Bell, D.R., Rossman, G.R., Winkler, B., 1991. The hydroxide component in synthetic pyrope. Am. Mineral. 76, 49–59.

Griffin, W.L., Jensen, B.B., Misra, S.N., 1971. Anomalously elongated rutile in eclogite-facies pyroxene and garnet. Nor. Geol. Tidsskr. 51, 177–185.

Gunther, M., Jagoutz, E., 1997. The meaning of Sm/Nd apparent ages from kimberlite-derived, coarse grained low temperature garnet peridotites from Yakutia. Russ. Geol. Geophys. 38, 229–239.

Haggerty, S.E., 1991. Oxide mineralogy of the upper mantle. In: Lindsley, D.H. (Ed.), Oxide Minerals: Petrologic and Magnetic Significance. Reviews in Mineralogy, vol. 25, pp. 355–416.

Haggerty, S.E., Sautter, V., 1990. Ultradeep (greater than 300 kilometers), ultramafic upper mantle xenoliths. Science 248, 993–996.

Hunter, W.C., Smith, D., 1981. Garnet peridotite from Colorado Plateau ultramafic diatremes: hydrates, carbonates, and comparative geothermometry. Contrib. Mineral. Petrol. 76, 312–320.

Irifune, T., 1987. An experimental investigation of the pyroxene–garnet transformation in a pyrolite composition and its bearing on the constitution of the mantle. Phys. Earth Planet. Inter. 45, 324–336.

Jarosewich, E., Nelen, J.A., Norber, J.A., 1980. Reference samples for electron microprobe analysis. Geostand. Newsl. 4, 43–47.

Jarosewich, E., Gooley, R., Husler, J., 1987. Chromium augite—a new microprobe reference sample. Geostand. Newsl. 11, 197–198.

Kennedy, C.S., Kennedy, G.C., 1976. The equilibrium boundary between graphite and diamond. J. Geophys. Res. 81, 2467–2470.

Krogh Ravna, E.K., 2000. The garnet–clinopyroxene Fe^{2+}–Mg geothermometer: an updated calibration. J. Metamorph. Geol. 18, 211–219.

Laz'ko, E.E., 1979. Diamond Indicator Minerals and Genesis of Kimberlite. Nedra Publications, Moscow. 192 pp.

Macdougall, J.D., Haggerty, S.E., 1999. Ultradeep xenoliths from African kimberlites: Sr and Nd isotopic compositions suggest complex history. Earth Planet. Sci. Lett. 170, 73–82.

Matsyuk, S.S., Langer, K., Hosch, A., 1998. Hydroxyl defects in garnets from mantle xenoliths in kimberlites of the Siberian platform. Contrib. Mineral. Petrol. 132, 163–179.

McCulloch, M.T., 1986. Sm–Nd systematics in eclogite and garnet peridotite nodules from kimberlites: implications for the early differentiation of the earth. In: Ross, J. (Ed.), Their Mantle/Crust Setting, Diamonds and Diamond Exploration. Kimberlites and Related Rocks, vol. 2. Blackwell Scientific Publications, Carlton, Australia, pp. 864–876.

Mitchell, R.H., 2004. Experimental studies at 5–12 GPa of the Ondermatjie hypabyssal kimberlite. Lithos 76, 551–564.

Moore, R.O., Gurney, J.J., 1985. Pyroxene solid solution in garnets included in diamond. Nature 318, 553–555.

Morimoto, N., Fabries, J., Ferguson, A.K., Ginzburg, I.V., Ross, M., Seifert, F.A., Zussman, J., Aoki, K., Gottardi, G., 1988. Nomenclature of pyroxenes. Am. Mineral. 73, 1123–1133.

Ono, S., Yasuda, A., 1996. Compositional change of majoritic garnet in a MORB composition from 7 to 17 GPa and 1400 to 1600 °C. Phys. Earth Planet. Inter. 96, 171–179.

Pearson, D.G., Shirey, S.B., Carlson, R.W., Boyd, F.R., Pokhilenko, N. P., Sobolev, N., 1995. Re–Os, Sm–Nd, and Rb–Sr isotope evidence for thick Archaean lithospheric mantle beneath the Siberian craton modified by multistage metasomatism. Geochim. Cosmochim. Acta 59, 959–977.

Pearson, D.G., Kelley, S.P., Pokhilenko, N.P., Boyd, F.R., 1997. Laser $^{40}Ar/^{39}Ar$ dating of phlogopites from southern African and Siberian kimberlites and their xenoliths: constraints on eruption ages, melt degassing and mantle volatile compositions. Russ. Geol. Geophys. 38, 106–117.

Roden, M.F., Shimizu, N., 1993. Ion microprobe analyses bearing on the composition of the upper mantle beneath the basin and range and Colorado Plateau provinces. J. Geophys. Res. 98 B, 14091–14108.

Roden, M.F., Laz'ko, E.E., Jagoutz, E., 1999. The role of garnet pyroxenites in the Siberian lithosphere: evidence from the Mir kimberlite. In: Gurney, J.J., et al. (Ed.), Proceedings of the 7th International Kimberlite Conference, Cape Town, vol. 2, pp. 714–720.

Sautter, V., Haggerty, S.E., Field, S., 1991. Ultradeep (>300 kilometers) ultramafic xenoliths: petrologic evidence from the transition zone. Science 252, 827–830.

Smith, D., 1999. Temperatures and pressures of mineral equilibration in peridotite xenoliths: review, discussion, and implications. In: Fei, Y., Bertka, C.M., Mysen, B.O. (Eds.), Mantle Petrology: Field Observations and High Pressure Experimentation: A Tribute to Francis R. Boyd. The Geochemical Soc., Spec. Pub., vol. 6, pp. 171–188. Houston.

Sobolev, N.V., 1977. Deep-Seated Inclusions in Kimberlites and the Problem of the Composition of the Upper Mantle. American Geophysical Union, Washington. 279 pp.

Sobolev, N.V., Lavrent'ev, J.G., 1971. Isomorphic sodium admixture in garnets formed at high pressures. Contrib. Mineral. Petrol. 31, 1–12.

Sobolev, N.V., Logvinova, A.M., Zedgenizov, D.A., Seryotkin, Y.V., Yefimova, E.S., Floss, C., Taylor, L.A., 2004. Mineral inclusions in microdiamonds and macrodiamonds from kimberlites of Yakutia: a comparative study. Lithos 77, 225–242.

Song, S., Zhang, L., Niu, Y., 2004. Ultra-deep origin of garnet peridotite from the North Qaidam ultrahigh-pressure belt, northern Tibetan Plateau, NW China. Am. Mineral. 89, 1330–1336.

Stein, C., 1995. Heat flow of the earth. In: Ahrens, T.J. (Ed.), Global Earth Physics, A Handbook of Physical Constants. American Geophysical Union, Washington, pp. 144–158.

Thompson, R.N., 1975. Is upper-mantle phosphorous contained in sodic garnet? Earth Planet. Sci. Lett. 26, 417–424.

Turcotte, D.L., Schubert, G., 2002. Geodynamics, 2nd edition. Cambridge University Press, Cambridge. 456 pp.

Van Orman, J.A., Grove, T.L., Shimizu, N., Layne, G.D., 2002. Rare earth element diffusion in a natural pyrope single crystal at 2.8 GPa. Contrib. Mineral. Petrol. 142, 416–424.

Van Roermund, H.L.M., Drury, M.R., 1998. Ultra-high pressure (P>6 GPa) garnet peridotites in western Norway: exhumation of mantle rocks from >185 km depth. Terra Nova 10, 295–301.

Van Roermund, H.L.M., Drury, M.R., Barnhoorn, A., De Ronde, A., 2000a. Non-silicate inclusions in garnet from an ultra-deep orogenic peridotite. Geol. J. 35, 209–229.

Van Roermund, H.L.M., Drury, M.R., Barnhoorn, A., De Ronde, A., 2000b. Super-silicic garnet microstructures from an orogenic garnet peridotite, evidence for an ultra-deep (>6 GPa) origin. J. Metamorph. Geol. 18, 135–147.

Van Roermund, H.L.M., Drury, M.R., Barnhorn, A., De Ronde, A., 2001. Relict majoritic garnet microstructures from ultra-deep orogenic peridotites in western Norway. J. Petrol. 42, 117–130.

Walther, M.J., 1998. Melting of garnet peridotite and the origin of komatiite and depleted lithosphere. J. Petrol. 39, 29–60.

Wang, L., Essene, E.J., Zhang, Y., 1999. Mineral inclusions in pyrope crystals from Garnet Ridge, Arizona, USA: implications for processes in the upper mantle. Contrib. Mineral. Petrol. 135, 164–178.

Wyatt, B.A., Baumgartner, M., Anckar, E., Grutter, H., 2004. Compositional classification of "kimberlitic" and "non-kimberlitic" ilmenite. Lithos 77, 819–840.

Yasuda, A., Fujii, T., 1994. Melting phase relations of an anhydrous mid-ocean ridge basalt from 3 to 20 GPa: implications for the behavior of subducted oceanic crust in the mantle. J. Geophys. Res. 99 B, 9401–9414.

Ye, K., Cong, B., Ye, D., 2000. The possible subduction of continental material to depths greater than 200 km. Nature 407, 734–736.

Zhang, R.Y., Liou, J.G., 2003. Clinopyroxenite from the Sulu ultrahigh-pressure terrane, eastern China: origin and evolution of garnet exsolution in clinopyroxene. Am. Mineral. 88, 1591–1600.

Zhang, R.Y., Zhai, S.M., Fei, Y.W., Liou, J.G., 2003. Titanium solubility in coexisting garnet and clinopyroxene at very high pressure: the significance of exsolved rutile in garnet. Earth Planet. Sci. Lett. 216, 591–601.

Zhuralev, A.Z., Laz'ko, E.E., Ponomarenko, A.I., 1991. Radiogenic isotopes and REE in garnet peridotite xenoliths from the Mir kimberlite pipe, Yakutia. Geochimiya 7, 982–994 (in Russian).